Microelectronics Journal, 26 (1995) 217–233

Review paper

Device modelling for the 1990s

H. Kosina, E. Langer and S. Selberherr

Institute for Microelectronics, Technical University of Vienna, Gußhausstraße 27–29, A-1040 Vienna, Austria. E-mail: kosina@iue.tuwien.ac.at

As semiconductor technology continues to evolve, numerical modelling of the devices' electrical behaviour is becoming increasingly important. In this contribution, the model hierarchy which exists for the description of current flow in a semiconductor device is briefly reviewed. The strengths and restrictions of each model are critically examined. Presently, drift-diffusion based simulation programs are considered as the workhorse tools in engineering. However, an enormous research effort is going on, with the aim of improving alternatives such as the hydrodynamic model, the spherical harmonics expansion method and the Monte Carlo technique. Examples of recently proposed improvements in that field are described.

1. Introduction

Since 1960, when demonstration of the practically usable MOS transistor first took place [1], its development has been rapid. Today, about 30 years later, integrated circuits with millions of devices per single chip are manufactured. To minimize the number of cycles of trial and error in device development, an improved understanding of basic device operation has attained a crucial importance. To meet these needs, many computer aids have been developed. Programs such as MINIMOS [2] and PISCES [3] are now essential tools for the device engineer.

Progress in photolithography and dry etching techniques have made it possible to define submicron horizontal features on semiconductor wafers. Concurrently, low-thermal-budget processes allow junction depths of the order of 10 nm to be achieved. This miniaturization necessitates an improvement in computer modelling of the electrical characteristics of small devices.

On one hand, certain device structures require three-dimensional models to address geometry-dependent effects [4–9]. On the other hand, today's devices are characterized by large electric fields in conjunction with steep gradients of the electric field and of the carrier concentrations. In many cases, the distances over which the variations occur are comparable to the carrier's mean free path. Under these conditions, the widely used drift-diffusion model is losing validity.

More sophisticated device models, such as the hydrodynamic and energy-transport models [9–15], the spherical harmonics expansion method [16–19] and the Monte Carlo technique [20–24], overcome these limitations. However, the increased physical rigour of a model comes at the expense of increased CPU times. This is a critical issue in particular for industrial sites. The efficiency of a device model determines whether it can be extensively applied in device optimization.

In this paper, we briefly review the state-of-the-art of the above-mentioned transport models. In particular, we present improvements of these models as they have been recently proposed in the literature.

0026–2692/95/$7.00 © 1995 Elsevier Science Ltd

All these models are based on the semiclassical Boltzmann transport equation (BTE):

$$\frac{\partial f}{\partial t} + \boldsymbol{u} \cdot \mathrm{grad}_r f + \frac{\boldsymbol{F}}{\hbar} \cdot \mathrm{grad}_k f = \left(\frac{df}{dt}\right)_{\mathrm{coll}} \tag{1}$$

where the unknown $f = f(\boldsymbol{k}, \boldsymbol{r}, t)$ is the distribution function. $\boldsymbol{F}$ denotes the external force field acting on the carriers. The collision term in (1) has the form of an integral operator:

$$\left(\frac{df}{dt}\right)_{\mathrm{coll}} = \int S(\boldsymbol{k}', \boldsymbol{k}) \cdot f(\boldsymbol{k}', \boldsymbol{r})\, d^3 k' - f(\boldsymbol{k}, \boldsymbol{r}) \cdot \int S(\boldsymbol{k}, \boldsymbol{k}')\, d^3 k' \tag{2}$$

the kernel of which is given by the differential scattering probability $S(\boldsymbol{k}, \boldsymbol{k}')$. A discussion of the BTE can be found elsewhere [25, 26].

Equation (1) is a time-dependent partial integro-differential equation in the six dimensional phase space $(\boldsymbol{k}, \boldsymbol{r})$. By the so-called 'method of moments' [27], this equation can be reduced to an infinite series of equations, in which the $\boldsymbol{k}$-dependence is eliminated. Keeping just the zero and first order moment equations, in conjunction with proper closure assumptions, leads to the basic semiconductor equations described in the next section. Accounting for one more moment yields the hydrodynamic model, which can be found in Section 3. Section 4 deals with the Monte Carlo method, a numerical method that solves (1) in a statistical manner.

2. Drift-diffusion based device models

Device modelling based on the self-consistent solution of the fundamental semiconductor equations dates back to the famous work of Gummel in 1964 [28]. Up to now, most of the device simulation tools used solve this set of equations.

2.1 The basic semiconductor equations

The well known fundamental semiconductor equations consist of Poisson's equation (3), continuity equations for electrons and holes (4), (5), and the current relations for both carrier types (6), (7):

$$\mathrm{div}\,(\varepsilon \cdot \mathrm{grad}\,\psi) = -\rho \tag{3}$$

$$\mathrm{div} \boldsymbol{J}_n - q \cdot \frac{\partial n}{\partial t} = q \cdot R \tag{4}$$

$$\mathrm{div} \boldsymbol{J}_p + q \cdot \frac{\partial p}{\partial t} = -q \cdot R \tag{5}$$

$$\boldsymbol{J}_n = q \cdot \mu_n \cdot \left(-n \cdot \mathrm{grad}\,(\psi) + \frac{k_B \cdot T_L}{q} \cdot \mathrm{grad}\,(n)\right) \tag{6}$$

$$\boldsymbol{J}_p = q \cdot \mu_p \cdot \left(-p \cdot \mathrm{grad}\,(\psi) - \frac{k_B \cdot T_L}{q} \cdot \mathrm{grad}\,(p)\right) \tag{7}$$

Here all symbols have their usual meaning [26]. In the literature, it is often argued that because of the occurrence of the lattice temperature T_L instead of individual carrier temperatures, these equations neglect any hot carrier effects. This argument is certainly true for the diffusive term. However, a realistic mobility model has to account for a mobility reduction at higher electric fields, and for many materials even velocity saturation can be assumed. From higher order transport models, we know that such a deviation from the ohmic low-field mobility is caused by heated carrier distribution functions. Therefore, through a realistic mobility model an essential hot carrier effect is introduced into the drift-diffusion equations. Impact ionization can be considered as another hot carrier effect that can be accounted for phenomenologically in these equations.

The development of proper models for the various coefficients made it possible to extend

the range in which reliable results can be obtained by solving the basic semiconductor equations.

2.2 Modelling mobilities

The models for the carrier mobilities have to account for various scattering mechanisms. In the following, the material under consideration is silicon.

In semiconductor devices, mobility reduction due to scattering on ionized impurities is a dominant effect. A well established procedure is to take the functional form (8) of the fit provided by Caughey and Thomas [29] and use temperature dependent coefficients:

$$\mu_{n,p}^{LI} = \mu_{n,p}^{\min} + \frac{\mu_{n,p}^{L} - \mu_{n,p}^{\min}}{1 + \left(\frac{CI}{C_{n,p}^{\mathrm{ref}}}\right)^{\alpha_{n,p}}} \tag{8}$$

Here μ_n^L, μ_p^L stand for the ohmic mobilities of the pure semiconductor. Values for all the parameters in the mobility expressions of this section, together with proper models for their temperature dependence, can be found elsewhere [30]. Due to partial ionization of impurity centres, one might also consider neutral impurity scattering. However, since there is some uncertainty about the quantitative values for ionized impurity scattering, it seems questionable to introduce another scattering mechanism with additional free parameters.

The electrical characteristic of a MOSFET is strongly influenced by surface scattering. An expression verified against measurements reads [30]

$$\mu_{n,p}^{LIS} = \frac{\mu_{n,p}^{\mathrm{ref}} + (\mu_{n,p}^{LI} - \mu_{n,p}^{\mathrm{ref}}) \cdot (1 - F(y))}{1 + F(y) \cdot \left(\frac{S_{n,p}}{S_{n,p}^{\mathrm{ref}}}\right)^{\gamma_{n,p}}} \tag{9}$$

The depth dependence is given by

$$F(y) = \frac{2 \cdot \exp(-(y/y^{\mathrm{ref}})^2)}{1 + \exp(-2 \cdot (y/y^{\mathrm{ref}})^2)} \tag{10}$$

The depth parameter y^{ref} is typically 10 nm. The pressing forces S_n and S_p are equal to the magnitude of the normal field strength at the interface, if the carriers are attracted by it, or zero, if the carriers are pushed away.

Mobility reduction caused by the electric field can be well approximated by the expressions

$$\mu_n^{LISF} = \frac{2\mu_n^{LIS}}{1 + \sqrt{1 + \left(\frac{2 \cdot \mu_n^{LIS} \cdot F_n}{v_n^{\mathrm{sat}}}\right)^2}},$$

$$\mu_p^{LISF} = \frac{\mu_p^{LIS}}{1 + \frac{\mu_p^{LIS} \cdot F_p}{v_p^{\mathrm{sat}}}} \tag{11}$$

where F_n and F_p are the effective driving forces defined as

$$F_n = \left| \mathrm{grad}\,\psi - \frac{1}{n} \cdot \mathrm{grad}\,(n \cdot U_{T_n}) \right|,$$

$$F_p = \left| \mathrm{grad}\,\psi + \frac{1}{p} \cdot \mathrm{grad}\,(p \cdot U_{T_p}) \right| \tag{12}$$

In the high field limit, this model yields saturated velocities, v_n^{sat} and v_p^{sat}. Expressions (11) reproduce experimental data well [31–33].

2.3 Modelling generation/recombination

The carrier generation/recombination term at the right-hand side of the carrier continuity equations comprises several mechanisms.

An adequate model for thermal generation/recombination is given by the well-known

Shockley–Read–Hall term [26]

$$R^{\mathrm{SRH}} = \frac{n \cdot p - n_i^2}{\tau_p \cdot (n + n_1) + \tau_n \cdot (p + p_1)} \tag{13}$$

with

$$n_1 = n_0 \cdot \frac{1 - f_{t0}}{f_{t0}}, \quad p_1 = p_0 \cdot \frac{f_{t0}}{1 - f_{t0}} \tag{14}$$

and the doping dependent carrier life times

$$\tau_n = \frac{\tau_{n0}}{1 + \dfrac{N_D + N_A}{N_n^{\mathrm{ref}}}}, \quad \tau_n = \frac{\tau_{p0}}{1 + \dfrac{N_D + N_A}{N_p^{\mathrm{ref}}}} \tag{15}$$

In (14) f_{t0} denotes the fraction of occupied traps in equilibrium, and n_0 and p_0 are the equilibrium carrier concentrations. The doping dependent empirical model for the carrier lifetimes (15) accounts for additional generation/recombination centres at high doping. The parameters are chosen to fit experimental findings [34].

Auger recombination is modelled by

$$R^{\mathrm{AU}} = (C_{cn} \cdot n + C_{cp} \cdot p) \cdot (n \cdot p - n_i^2) \tag{16}$$

with appropriate temperature dependent Auger coefficients [35].

As a model for impact ionization, the Chynoweth formulation (17) can be used. Although the actuality of this model [36] has been much discussed in the scientific community, it still seems that it fulfils the requirements for device simulation quite satisfactorily:

$$\alpha_{n,p} = \alpha_{n,p}^{\infty} \cdot \exp\left(-\frac{\beta_{n,p}}{E}\right) \tag{17}$$

The ionization coefficients then determine the generation rate according to

$$-R^{\mathrm{II}} = \alpha_n \cdot \frac{|\boldsymbol{J}_n|}{q} + \alpha_p \cdot \frac{|\boldsymbol{J}_p|}{q} \tag{18}$$

The coefficients of (17) can be modelled temperature dependent to fit experimental data [37–39]. A comparison to other models for impact ionization can be found elsewhere [40]. The scatter among the results of the different models indicates that more effort is necessary in this area to better understand impact ionization, and to obtain a more rigorous description of this phenomenon.

3. The hydrodynamic model

The hydrodynamic approach extends beyond the drift-diffusion approach by allowing the carrier temperatures to differ from the lattice temperature. Furthermore, coefficients such as mobilities and ionization coefficients can be functions of some higher order moments [41, 42].

3.1 The basic equations

In the following, we briefly summarize the basic equations of the hydrodynamic model. Poisson's and carrier continuity equations (3)–(5) retain their validity. In contrast to the drift-diffusion model, additional moment equations are now included, accounting for second order moments

$$\frac{\partial(n \cdot w_n)}{\partial t} + \mathrm{div}\, \boldsymbol{S}_n = \boldsymbol{E} \cdot \boldsymbol{J}_n - R \cdot w_n - n \cdot \frac{w_n - w_0}{\tau_{wn}} \tag{19}$$

$$\frac{\partial(p \cdot w_p)}{\partial t} + \mathrm{div}\, \boldsymbol{S}_p = \boldsymbol{E} \cdot \boldsymbol{J}_p - R \cdot w_p - p \cdot \frac{w_p - w_0}{\tau_{wp}} \tag{20}$$

These equations imply continuity of the energy fluxes $\boldsymbol{S}_n$ and $\boldsymbol{S}_p$, for both the electron and hole distributions. Here τ_{wn} and τ_{wp} are the respective energy relaxation times, and w_0 is the average energy in thermodynamic equilibrium. The average carrier energies w_n, w_p are related to the average velocities v_n, v_p and the hydrodynamic temperatures T_n, T_p by

$$w_n = \frac{1}{2} \cdot m_n^* \cdot v_n^2 + \frac{3}{2} \cdot k_B \cdot T_n \tag{21}$$

$$w_p = \frac{1}{2} \cdot m_p^* \cdot v_p^2 + \frac{3}{2} \cdot k_B \cdot T_p \tag{22}$$

The energy fluxes have the form

$$\boldsymbol{S}_n = \mathbf{Q}_n - (w_n + k_B \cdot T_n) \cdot \frac{\boldsymbol{J}_n}{q} \tag{23}$$

$$\boldsymbol{S}_p = \mathbf{Q}_p + (w_p + k_B \cdot T_p) \cdot \frac{\boldsymbol{J}_p}{q} \tag{24}$$

Critical remarks on, for example, modelling the heat fluxes $\mathbf{Q}_n$, $\mathbf{Q}_p$ are made later in this section. Compared with (6) and (7), in the hydrodynamic model the current relations are more complex:

$$\boldsymbol{J}_n - \frac{\tau_{pn}}{q} \cdot (\boldsymbol{J}_n \cdot \mathrm{grad}) \frac{\boldsymbol{J}_n}{n} = q \cdot \mu_n \cdot \left(-n \cdot \mathrm{grad}\,(\psi) + \mathrm{grad}\left(n \cdot \frac{k_B \cdot T_n}{q} \right) \right) \tag{25}$$

$$\boldsymbol{J}_p + \frac{\tau_{pp}}{q} \cdot (\boldsymbol{J}_p \cdot \mathrm{grad}) \frac{\boldsymbol{J}_p}{p} = q \cdot \mu_p \cdot \left(-p \cdot \mathrm{grad}\,(\psi) - \mathrm{grad}\left(p \cdot \frac{k_B \cdot T_p}{q} \right) \right) \tag{26}$$

Before we describe the various models in more detail, let us consider some numerical aspects concerning the hydrodynamic approach. Difficulties arise from the increased stiffness of the momentum conservation equations (25) and (26). Furthermore, it is problematic to obtain a smooth discretized representation of the Joule heat $\boldsymbol{E} \cdot \boldsymbol{J}$, which appears in the energy balance equations. An attempt to relax this problem has recently been published [43]. A different interpretation of the energy flux yields a simpler heat generation term of the form $\mu \cdot \boldsymbol{F}^2$, where $\boldsymbol{F}$ is the driving force acting on the carriers. The advantages seem to be, first, that the vector components of $\boldsymbol{F}$ can be assembled more easily at each meshpoint than that of $\boldsymbol{J}$, and second, that a scalar product no longer has to be evaluated which sensitively depends upon the angle between the two vectors.

Discretization of the energy balance equations is by far more ambiguous than that of the carrier continuity equations. For this purpose, several attempts to generalize the Scharfetter–Gummel scheme have been proposed [44, 45].

It has been shown [46] that simulation of devices at 77K requires modifications of the discretization schemes of both the carrier- and energy balance equations. To avoid artificial driving forces in equilibrium, a distinction needs to be made between the hydrodynamic and thermodynamic temperatures.

We believe that there is still room for improvements of the discretization scheme for the hydrodynamic equations such that better convergence properties can be achieved.

3.2 Modelling relaxation times

In the following, we address models for energy relaxation times and mobilities. The latter are related to the momentum relaxation times by

$$\mu_n = \frac{q \cdot \tau_{pn}}{m_n^*}, \quad \mu_p = \frac{q \cdot \tau_{pp}}{m_p^*} \tag{27}$$

The first class of models, which is widely in use, assumes the relaxation time to be a function of the average energy w, as derived from the energy balance equation. Such an assumption is already sufficient to reproduce certain non-local transport phenomena such as velocity overshoot.

In [47], the distribution function is first expanded linearly into its first four moments. That Ansatz cannot only be used in the left-hand side of the BTE (1), but also in the scattering integral at the right-hand side. Therefore, in addition to a set of moment equations, one can also obtain information about material characteristics. Mobility and energy relaxation time turn out to be the following functions of the moments:

$$\frac{1}{\mu_n} = a + b \cdot \frac{\boldsymbol{J}_n \cdot \boldsymbol{S}_n}{\boldsymbol{J}_n^2} \tag{28}$$

$$\tau_{wn} = \text{const} \tag{29}$$

where a and b are constant parameters with respect to the moments.

If the hydrodynamic equations are reduced to the homogeneous case, i.e. all spatial derivatives are set to zero, an energy dependent expression can be derived from (28):

$$\mu_n = \frac{\mu_0}{1 + \alpha \cdot (w_n - w_0)} \tag{30}$$

$$\alpha = \frac{\mu_0}{(q \cdot \tau_{wn} \cdot v_{n,\mathrm{sat}}^2)} \tag{31}$$

α contains parameters describing the asymptotic behaviour for small and large electric fields. Applications of (30) to the simulation of MOSFETs can be found elsewhere [48]. It should be noted that by means of the homogeneous hydrodynamic equations, the mobility after (30) can also be transformed into a field-dependent expression. The result is then identical with (11) used in the drift-diffusion equations.

A different approach was taken in [11]. A main assumption is that the diffusion coefficient can well be approximated by a constant. The generalized Einstein relation then reads

$$D_n = \frac{k_B \cdot T_n}{q} \cdot \mu(T_n) = \frac{k_B \cdot T_L}{q} \cdot \mu_0 \tag{32}$$

where μ_0 is the low-field mobility. In [11], this expression has been combined with the empirical Coughey–Thomas relation for the field-dependence of the mobility

$$\mu_n(E) = \mu_0 \cdot \left(1 + \left(\frac{\mu_0 \cdot E}{v_{n,\mathrm{sat}}}\right)^2\right)^{-1/2} \tag{33}$$

Exploiting the hydrodynamic equations for the homogeneous case, one obtains the final result

$$\mu_n(T_n) = \mu_0 \cdot \frac{T_L}{T_n} \tag{34}$$

$$\tau_{wn}(T_n) = \frac{m_n^* \cdot \mu_0}{2 \cdot q} \cdot \frac{T_L}{T_n} + \frac{3}{2} \cdot \frac{k_B \cdot \mu_0}{q \cdot v_{n,\mathrm{sat}}^2} \cdot \frac{T_n \cdot T_L}{T_n + T_L} \tag{35}$$

In that model, τ_{wn} exhibits a weak carrier temperature dependence.

Recently, mobility has been considered as the more fundamental quantity, which is no longer

discussed in terms of effective mass and momentum relaxation time, as stated by (27). There exists a more general definition which neither relies on the relaxation time approximation nor on the constant effective mass approximation:

$$q \cdot \boldsymbol{v} = \mu \cdot \left(\frac{d\boldsymbol{p}}{dt}\right)_{\text{coll}} \tag{36}$$

In this equation, μ relates the velocity to the average momentum loss rate. It has become common practice to calculate the macroscopic mobility according to (36) by means of a more rigorous transport model, e.g. the Monte Carlo method [49, 50] or the scattering matrix approach [51, 52]. This can even be done in a space dependent fashion for strong non-uniform conditions, as they are present in small devices. In that way, it has become possible to examine basic assumptions underlying the hydrodynamic model.

It has been investigated [50, 52] whether mobility is a function of the carrier energy in strongly inhomogeneous situations. In either of the works, an n^+–n–n^+ diode served as a test device, and the $\mu(w)$ dependence has been extracted from bulk simulations. It has been found that the use of $\mu(w)$ substantially overestimates the true mobility near the channel-drain junction, the reason being that in this region the distribution function differs significantly from the bulk distribution. The important observation is that the mobility is not a single-valued function of the carrier energy.

Moreover, it has been demonstrated [50] that the mobility model (28), originally derived by Hänsch [53], works very well in the inhomogeneous case. Instead of the carrier energy, both the drift-velocity and the energy flux are much better suited to reproduce the true mobility.

3.3 Modelling heat flux

A well known characteristic of the method of moments is that the moment equation of order i always contains an $(i+1)$th order moment. In the case of the energy balance equation, this next higher moment is of third order

$$\mathbf{Q}(\boldsymbol{r}) = \int \frac{m^*}{2} \cdot c(\boldsymbol{k})^2 \cdot \boldsymbol{c}(\boldsymbol{k}) \cdot f(\boldsymbol{k}, \boldsymbol{r})\, d^3 k \tag{37}$$

which has the physical meaning of a macroscopic heat flux density. Here $\boldsymbol{c}(\boldsymbol{k})$ denotes the random velocity defined as $\boldsymbol{c}(\boldsymbol{k}) = \boldsymbol{u}(\boldsymbol{k}) - \langle\boldsymbol{u}\rangle$. To close the set of moment equations, this higher order moment somehow has to be related to the lower order moments. For the heat flux one conventionally assumes Fourier's law

$$\mathbf{Q}(\boldsymbol{r}) = -\kappa(\boldsymbol{r}) \cdot \operatorname{grad} T(\boldsymbol{r}) \tag{38}$$

in conjunction with a generalized Wiedemann–Franz law

$$\kappa(\boldsymbol{r}) = \left(\frac{5}{2} + c'\right) \cdot \left(\frac{k_B}{q}\right)^2 \cdot \sigma(\boldsymbol{r}) \cdot T(\boldsymbol{r}) \tag{39}$$

for the thermal conductivity κ of the considered carrier gas.

Equation (38), however, cannot include the fact that $\mathbf{Q}$ may not be zero, even in a homogeneous system. If a uniform electric field is applied to a semiconductor, not only the distribution function of $\boldsymbol{u}$ becomes asymmetric, but also that of the random velocity $\boldsymbol{c}$. In that case, (37) yields a nonzero $\mathbf{Q}$.

To model the kinetic heat flux (37) more carefully, one can analyse the moment equation of third order [50, 54]. By comparing the various terms of the energy flux density, $\mathbf{Q}$ can be identified as

$$\mathbf{Q} = \mathbf{Q}_{\text{diff}} + \mathbf{Q}_{\text{conv}} \tag{40}$$

An additional convective component occurs, which has commonly been neglected in the hydrodynamic model in the past.

In [52], for a small, one-dimensional test structure, by means of a rigorous Boltzmann-solver, both expressions (37) and (38) have been evaluated and then compared. It has been shown that $\boldsymbol{Q}$ contributes significantly to the energy flux density $\boldsymbol{S}$, and, more importantly, Fourier's law is heavily in error. In the computer experiment reported, even a region with counter-gradient heat transport has been observed. As a model for the convective Peltier-like component, the following expression has been proposed:

$$\mathbf{Q}_{\text{conv}} = \frac{5}{2} \cdot \left(1 - \frac{\tau_s}{\tau_p}\right) \cdot \frac{k_B \cdot T}{q} \cdot \boldsymbol{J} \tag{41}$$

where τ_s stands for the energy flux relaxation time. For the diffusive component, Fourier's law can still be used, however, a modified thermal conductivity is suggested

$$\kappa = \frac{\tau_s}{\tau_p} \cdot \frac{5}{2} \cdot \left(\frac{k_B}{q}\right)^2 \cdot \sigma \cdot T \tag{42}$$

There have been ongoing discussions in the literature about the so-called 'spurious velocity overshoot'. This effect is a non-physical spike in the velocity profile, which is often predicted by the hydrodynamical model in simple n–i–n diodes. It has been argued that the erroneous heat flux given by Fourier's law is probably responsible for that non-physical spike.

3.4 Quantum mechanical extensions

The BTE (1) treats carriers as classical particles. As both $\boldsymbol{k}$ and $\boldsymbol{r}$ are specified simultaneously, Heisenberg's uncertainty principle is ignored. However, quantum mechanical effects play an important role for the function of many devices, e.g. through the inversion layer of a MOSFET, through the channels of modulation doped FETs and for the resonant tunneling diode. An equation capable of dealing with the wave nature of the carriers is the so-called Wigner–Boltzmann equation [55]. As it is accessible to the method of moments, a set of balance equations can be derived that incorporate first-order quantum corrections. The resulting $O(\hbar^2)$ terms allow particle tunneling through barriers and charge buildup in potential wells.

Following [56], such a procedure yields a set of equations very similar to the classical hydrodynamic equations described above. If we identify the term $n \cdot k_B \cdot T_n$ in (25) in accord with kinetic gas theory as the pressure P of the electron gas, then the quantum corrections turn out to change just the definitions of pressure and energy. The corrections have the form

$$P_{ij} = n \cdot k_B \cdot T_n \cdot \delta_{ij} - \frac{\hbar^2}{12 m_n^*} \cdot \frac{\partial^2}{\partial x_i \partial x_j} \cdot \ln(n) \tag{43}$$

$$w_n = \frac{1}{2} \cdot m_n^* \cdot v_n^2 + \frac{3}{2} \cdot k_B \cdot T_n - \frac{\hbar^2}{24 m_n^*} \cdot \Delta \ln(n) \tag{44}$$

In the limit $\hbar \to 0$ the classical hydrodynamic equations are recovered. An application of this model to a one-dimensional simulation of a resonant tunneling diode has been reported [56]. A two-dimension simulation of very small MESFETs can also be found [57].

4. The Monte Carlo method

In this section we describe a recently implemented hybrid approach that combines Monte Carlo and drift-diffusion analysis. In critical device regions, the position-dependent coefficients of an extended drift-diffusion equation are extracted from a Monte Carlo simulation.

Additional features which make the code more efficient are presented. A unique self-consistent iteration scheme has been developed which converges faster than all presently known schemes. It exploits the so-called Monte Carlo–Drift Diffusion coupling technique, which also forms the basis of the hybrid method. The simulator has been used to model submicron MOSFETs with gate lengths down to 0.15 μm. In addition to the non-local effects occurring in these devices, the performance of the hybrid simulation method is analysed.

4.1 Coupling the Monte Carlo and drift-diffusion models

The hybrid approach can be justified rigorously from the BTE, since either of the models to be coupled provide, certainly under different conditions, a solution to it [58].

From (1) one can directly derive the moment equation of first order:

$$q \cdot E_j + \frac{1}{n} \cdot \frac{\partial n \cdot <\hbar k_j \cdot v_k>}{\partial r_k} = -\left(\frac{dp_j}{dt}\right)_{\mathrm{coll}} \tag{45}$$

where the distribution function implied by the averages is still treated as an unknown function. Summation over repeated indices is assumed. Here, the right-hand side represents the average momentum loss rate, which explicitly reads as

$$\left(\frac{d\boldsymbol{p}}{dt}\right)_{\mathrm{coll}} = < \int (\hbar \boldsymbol{k} - \hbar \boldsymbol{k}')\, S(\boldsymbol{k}, \boldsymbol{k}')\, d^3k' > \tag{46}$$

If we insert the general mobility definition (36) into (45), and if we interpret the second moment as energy tensor,

$$w_{jk} = \frac{1}{2} \cdot <\hbar k_j \cdot v_k> \tag{47}$$

we end up with a current equation of the form

$$J_i = q \cdot n \cdot \mu_{ij} \cdot E_j + \mu_{ij} \cdot \frac{\partial}{\partial r_k} (2 \cdot w_{jk} \cdot n) \tag{48}$$

Due to the similarity of (48) and the conventional drift-diffusion equation, both equations comprise a drift and a diffusive term; we consider (48) as an extended drift-diffusion equation.

The Monte Carlo technique can now be used to calculate the coefficients μ_{ij} and w_{ij} according to (36) and (47), respectively. By using these coefficients in (48), the link between the Monte Carlo particle model and the extended drift-diffusion equation is established.

The derivation of the coupling coefficients from the moments outlined above shows the generality of this method. All the physical models affecting the distribution function which are accounted for in the Monte Carlo simulator (e.g. band-structure models or scattering processes) directly influence the moments, and thus the coupling coefficients. From a theoretical point of view, in addition to the approximations inherent to the Monte Carlo model, no further approximation is introduced when the Monte Carlo model is coupled with (48).

Under conditions far from thermal equilibrium, (48), together with Monte Carlo generated space-dependent coefficients, simply reproduce the Monte Carlo current density. Approaching thermal equilibrium, the energy tensor becomes independent of space, and is solely determined by the lattice temperature, and μ reverts to the low-field mobility μ_0. In this manner, the conventional drift-diffusion equation is recovered. The set of semiconductor equations incorporating the extended drift-diffusion equation (48) is therefore capable of describing high-energy transport as well as low-field transport in very small devices.

For numerical implementation it is desirable to have isotropic coefficients in the current

relation. In this work, isotropic temperature and mobility are obtained by the following approximations of the tensors:

$$\mu = q \cdot \sqrt{\frac{<\boldsymbol{v}>^2}{(d\vec{\boldsymbol{p}}/dt)_c^2}} \tag{49}$$

$$T = \frac{2}{k_B} \cdot \frac{1}{N} \cdot \sum_{i=1}^{N} w_{ii} \tag{50}$$

N is the number of considered space dimensions.

4.2 A new self-consistent iteration scheme

For very short devices, an increasing fraction of the electron population is in non-equilibrium conditions. As Monte Carlo treats the average motion of those electrons in a way which differs substantially from a standard drift-diffusion model, the resultant distribution of mobile charge in real space will also differ. Realistic results can therefore only be expected by applying some sort of self-consistent technique. The standard technique [59] couples the BTE solved by the Monte Carlo method with a linear Poisson equation. This method, though straightforward, may lead to stability problems. Improvements are obtained by a non-linear coupling scheme [22].

On the basis of the Monte Carlo–drift-diffusion coupling method, a novel self-consistent solution strategy can be investigated. Let us consider the following set of equations:

$$\text{div}\,(\varepsilon \cdot \text{grad}\,\psi) = q \cdot (n - p - N_C) \tag{51}$$

$$\text{div}\,\boldsymbol{J} = 0 \tag{52}$$

$$\boldsymbol{J} = q \cdot n \cdot \mu \cdot \left(\boldsymbol{E} + \frac{1}{n} \cdot \text{grad}\,(n \cdot U_T)\right) \tag{53}$$

which includes the extended drift-diffusion equation. The latter is obtained from (48) if the isotropic coefficients are inserted. We have introduced the temperature voltage related to the carrier temperature by

$$U_T = \frac{k_B \cdot T}{q} \tag{54}$$

In each cycle of the self-consistent iteration loop, a Monte Carlo simulation has to be performed, the potential for which is taken from the previous cycle, and the distributions of μ and U_T serve as the result. Then the critical device regions are identified by certain criteria [24]. These coefficients, taken from Monte Carlo just in the critical device regions, are then extended analytically over the rest of the simulation domain. With the μ and U_T profiles assembled in such a way, the coupled set of equations, (51), (52) and (53), is solved. With the updated potential the iteration cycle is repeated until the change in the potential is sufficiently small. Figure 1 shows a flowchart of this algorithm. The initial potential distribution, $\psi^{(0)}$, is generated by a standard drift-diffusion simulation.

This new approach to self-consistency is expected to yield a high convergence rate. Generally, the carrier concentration is quite sensitive to small changes in the potential, due to the roughly exponential dependence. On the other hand, the potential strongly depends upon the space-charge density, which is determined by the carrier concentration. A procedure that iteratively calculates ψ from n (solving Poisson's equation) and then n from ψ (solving the transport problem) will suffer from this strong coupling, and will thus exhibit a slow convergence rate.

Considering the coefficients used in our iteration scheme, we find that they depend upon some kind of first order moments, $<\boldsymbol{v}(\boldsymbol{k})>$, $(dp/dt)_c$, and on the second order moment, $<\hbar k_i \cdot v_j(\boldsymbol{k})>$, but that they definitely do not depend upon the zero-order moment, $n(\mathbf{r})$. The critical potential dependence as it exists for $n(\mathbf{r})$ is thus removed

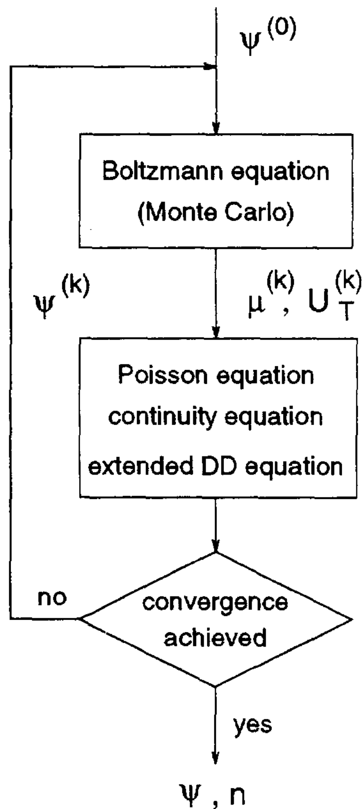

Fig. 1. Flowchart of the self-consistent iteration scheme.

from the coupling coefficients. Consequently, there is just a quite moderate coupling between the iterated quantities, ψ and (μ, U_T) (see Fig. 1). This explains the extremely low number of iterations required, as demonstrated next.

4.3 Results

We have applied the hybrid technique to the simulation of n-channel MOS-devices. Gate mask length ranges from 0.75 μm down to 0.15 μm. Table 1 summarizes the characteristic parameters of the devices under investigation. L_{eff} denotes the distance between the vertical pn-junctions, r_j is the junction depth and t_{ox} is the oxide thickness. The threshold voltage, V_{TH}, is determined at room temperature for $V_{\mathrm{DS}} = 0.05$ V. For devices A and B, doping

TABLE 1 Characteristic parameters of the simulated n-channel MOSFETs

Device	L_G (μm)	L_{eff} (μm)	r_j (μm)	t_{ox} (nm)	V_{DS} (V)	U_{TH} (V)
A	0.15	0.121	0.039	5	2.0	0.24
B	0.25	0.168	0.125	5	2.5	0.26
C	0.75	0.604	0.181	15	5.0	0.70

profiles are modelled with process parameters similar to those described elsewhere [60, 61].

The conduction band is assumed non-parabolic; models for scattering mechanism are taken from [62]. Throughout the simulations, for the non-parabolic correction we use $\alpha = 0.7$ eV^{-1}, $\Delta \cdot L = 0.3$ nm^2 (surface roughness parameter, see [63]) and $N = 5 \cdot 10^7$ as the number of scattering events to be calculated during a single Monte Carlo simulation.

Quantities such as drain current, drift velocity and carrier concentrations plotted in this section are obtained from a solution to the extended semiconductor equations, (51), (52) and (53).

Figure 2 shows the evolution of the drain current with the number of iterations for device

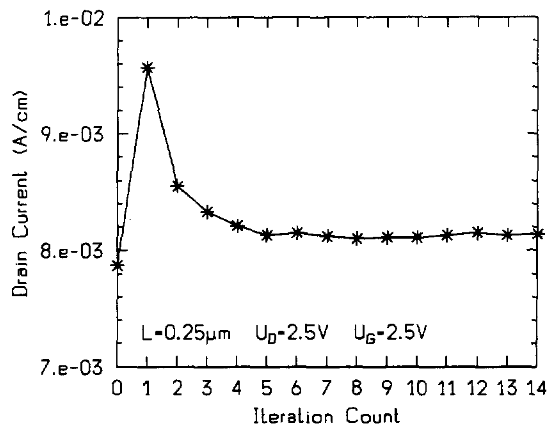

Fig. 2. Convergence rate of the self-consistent coupling scheme: drain current as a function of the number of iterations for device B at a high gate bias.

B. An iteration number of zero corresponds to the initial solution determined by a standard drift-diffusion simulation. The drastic increase in the drain current after the first iteration can be attributed to velocity overshoot. Subsequent iterations cause the impact of velocity overshoot on I_D to be reduced, so that the final stationary value of I_D lies slightly above $I_D^{(0)}$. In Figs. 3a and c the evolution of I_D is shown for the 0.75 μm device at different gate biases. In Fig. 3c, where $V_{GS} = V_{DS}$, an overshoot of I_D can be observed at the beginning of the iteration. Figures 3b and d show the relative norms of the increments of carrier concentration and electrostatic potential as a function of the number of iterations. The norms first decrease rapidly, but are then limited due to the statistical noise inherent in the Monte Carlo method. The relative norms of the ψ-increments typically taper off below 10^{-3}. In all the simulations we have performed, an iteration count no larger than five was required to obtain the final drain current. Any systematic transient in the relative norms also dies out within this iteration number. With the new iteration scheme, the number of costly Monte Carlo–Poisson iterations is considerably reduced

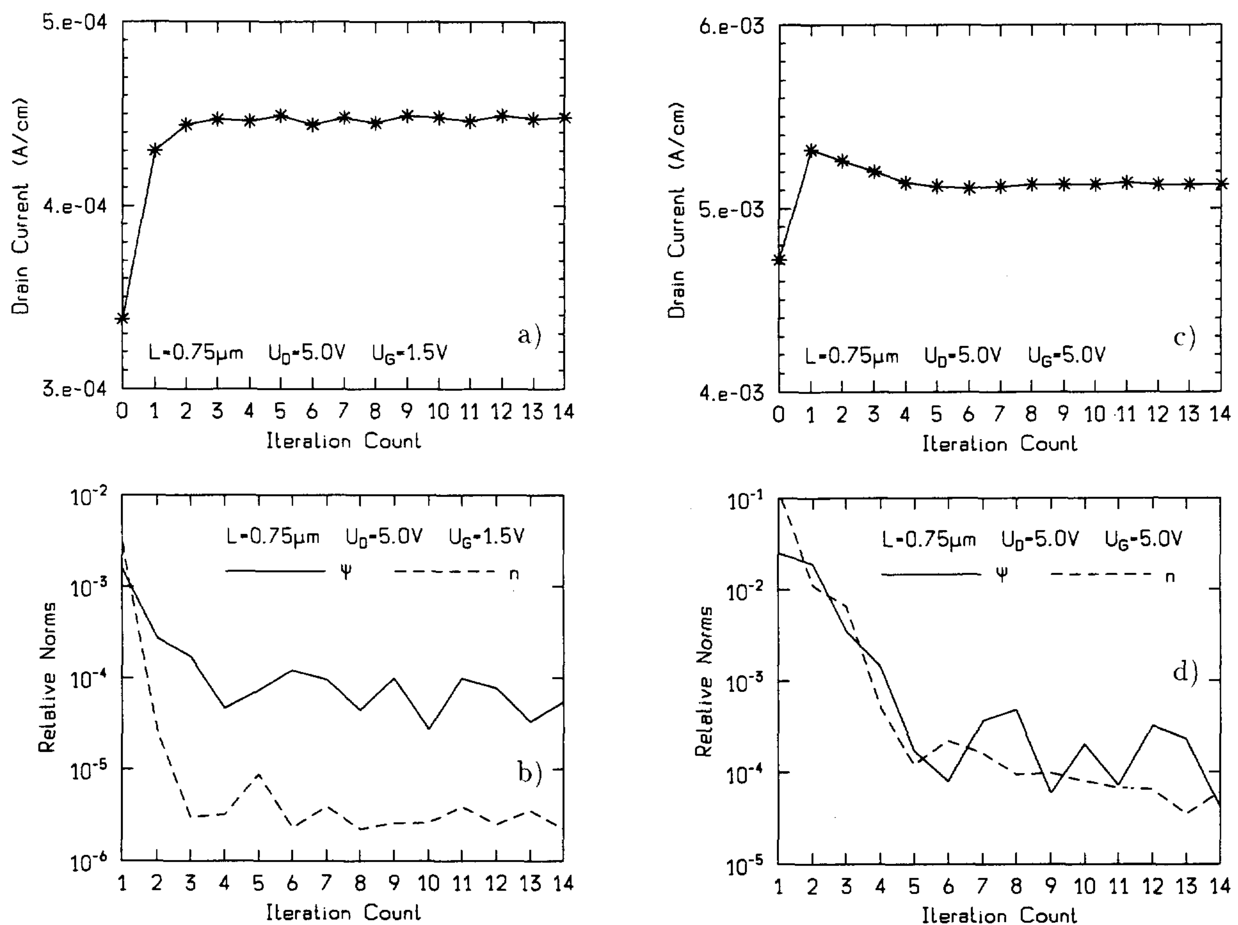

Fig. 3. Convergence rate of the self-consistent coupling scheme: drain currents and relative norms of the n- and ψ-increments as a function of the number of iterations for device C at different gate biases.

compared to other coupling schemes reported in the literature [22, 59].

To figure out the differences between self-consistent Monte Carlo and self-consistent drift-diffusion simulations, we have plotted the potential and the electric field occurring at the Si/SiO_2 interface of devices A and B in Fig. 4. In the Monte Carlo case, in the high field region the potential profile become smoother (Fig. 4a, c) so that a significant lower lateral electric field is predicted (Fig. 4b, d). This effect comes from a reduced space charge density in that area, as is indicated by the reduced carrier concentration shown in Fig. 6b. When using standard drift-diffusion simulations for such small devices, one should be aware first of the tendency to overestimate the maximum electric field by some 10% (e.g. 39% in device A, 35% in device B). Second, to predict hot carrier-induced phenomena such as impact ionization, the maximum electric field is not as significant as in long-channel devices. Due to the narrowness of the field peak, its capability of producing damage is decreased.

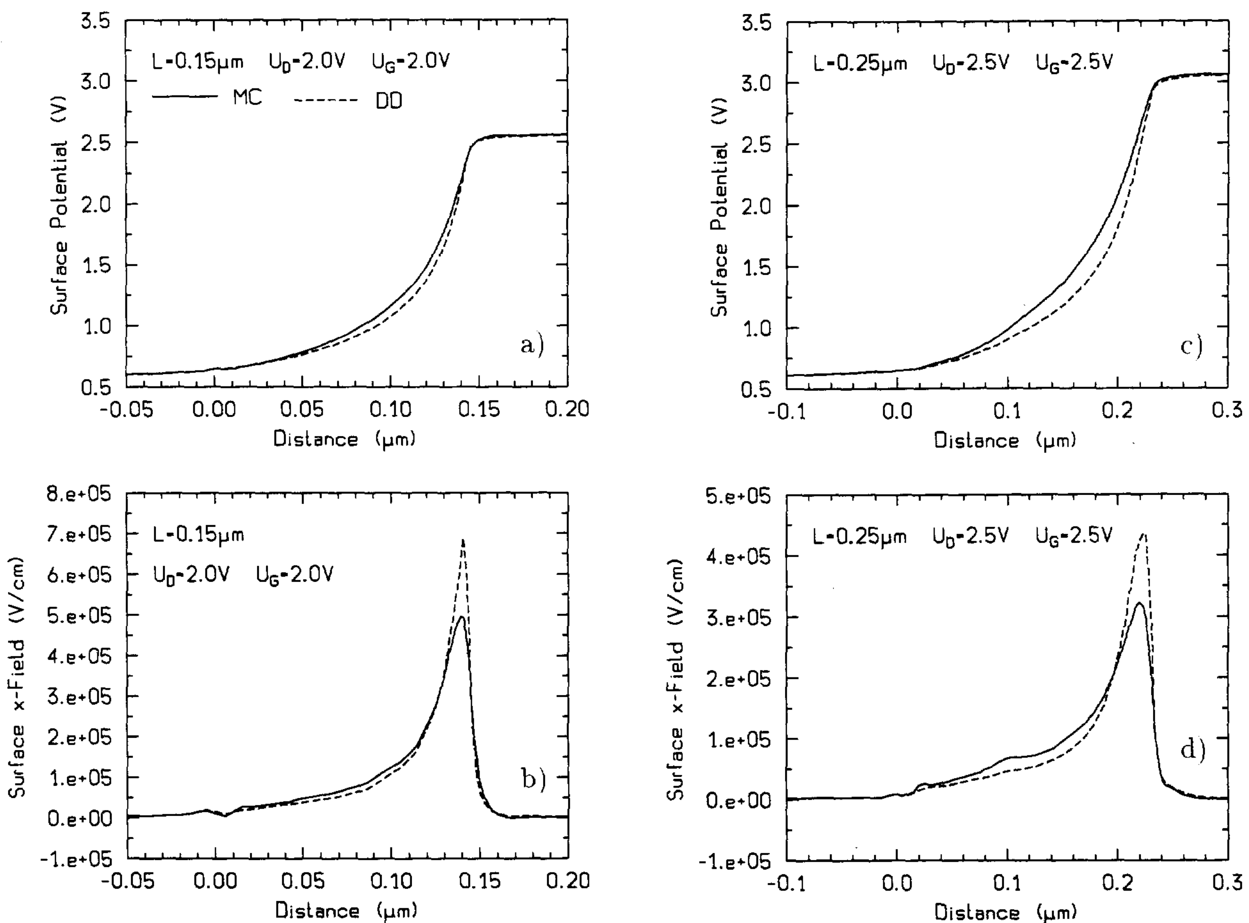

Fig. 4. Comparison of self-consistent DD (dashed line) and self-consistent MC (solid line) results for devices A and B. (a) and (b) surface potential; (c) and (d) lateral electric field at the surface.

In Fig. 5 we compare the surface mobility obtained from a local model with that from a Monte Carlo simulation. At the beginning and end of the depicted lateral distance, mobility is mainly determined by the high doping levels in that section.

In the high-field region, where the extended semiconductor equations massively reproduce velocity-overshoot (see Fig. 6a), the non-local mobility (solid line) exceeds the local one (dashed line). In the example shown in Fig. 5, the absolute minima differ by 37%. The local mobility recovers from its minimum to the same extent as the electric field decreases, whereas the non-local mobility, which is degraded due to a hot distribution function, recovers with some delay, since cooling has to take place.

As for Fig. 6a, the velocity profile from the local mobility model (dashed line) is clearly bounded by the bulk saturation velocity ($v_{sat} = 10^7$ cm/s). The reasons why the carrier concentrations in the non-local case (Fig. 6b) are lower than in the local case are twofold. First, due to the introduction of carrier heating, which is absent in the standard drift-diffusion model, the inversion layer broadens, and thus the surface concentration lowers. The second contribution comes from the continuity of the total current, which is controlled by the situation at the source-sided part of the channel. Velocity overshoot in this region is not very pronounced. In the pinch-off region, the massive overshoot in the velocity is then compensated for by an undershoot in the carrier concentration.

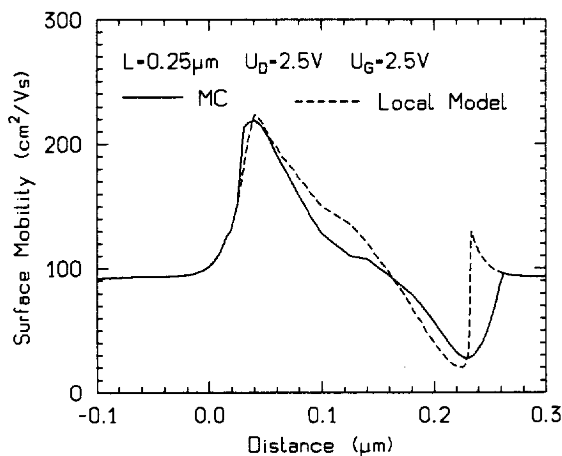

Fig. 5. Surface mobilities in device B for $V_G = V_D = 2.5$ V. Solid line: non-local mobility from a MC simulation. Dashed line: local (analytical) mobility model.

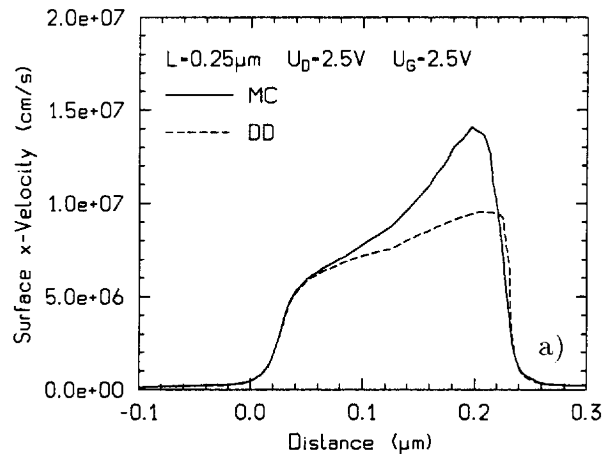

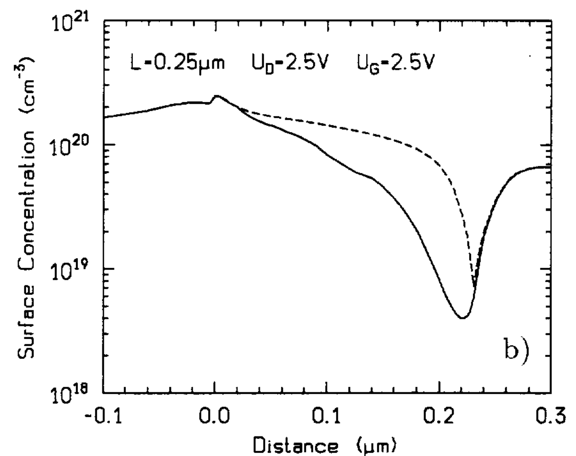

Fig. 6. Comparison of MC- (solid line) and DD-results (dashed line) for device B. (a) average velocity at the surface; (b) surface concentration of electrons.

5. Conclusion

Most of the device simulations carried out today are based on the drift-diffusion model. Carefully chosen models for the coefficients herein make it possible to obtain reliable results down to half-micron device sizes. Huge efforts are currently being made to improve the hydrodynamic and energy transport models. We have pointed out that basic assumptions such as an energy dependent mobility or Fourier's law for the heat flux can be in severe error in very small devices. Recently proposed improvements of both the physical models and the numerical techniques show us that with the hydrodynamic model, more accurate and probably more robust simulations become possible. Hybrid approaches have emerged, that combine computational efficiency with more demanding methods for the analysis of a single device. We have presented an implementation of such an approach connecting the Monte Carlo and the drift-diffusion models.

Acknowledgments

This work is supported by the laboratories of: Austrian Industries – AMS at Unterpremstätten, Austria; Digital Equipment Corporation at Hudson, USA and Siemens Corporation at Munich, Germany.

References

[1] D. Kahng and M.M. Atalla, Silicon–silicon dioxide field induced surface devices, *IRE-AIEE Solid-State Device Res. Conf.*, 1960.

[2] W. Hänsch and S. Selberherr, MINIMOS 3: A MOSFET simulator that includes energy balance, *IEEE Trans. Electron Dev.*, ED-34(5) (1987) 1074–1078.

[3] M.R. Pinto, *PISCES IIB*, Stanford University, 1985.

[4] P. Ciampolini, A. Pierantoni, M. Melanotte, C. Cecchetti, C. Lombardi and G. Baccarani, Realistic device simulation in three dimensions, *Proc. Int. Electron Devices Meeting*, 1989, 131–134.

[5] G. Heiser, C. Pommerell, J. Weis and W. Fichtner, Three-dimensional numerical semiconductor device simulation: algorithms, architectures, results, *IEEE Trans. Computer-Aided Design*, 10(10) (1991) 1218–1230.

[6] T.D. Linton and P.A. Blakey, A fast, general three-dimensional device simulator and its application in a submicron EPROM design study, *IEEE Trans. Computer-Aided Design*, CAD-8(5) (1989) 508–515.

[7] S. Selberherr and E. Langer, Three dimensional process and device modeling, *Microelectronics J.*, 20(1–2) (1989) 113–127.

[8] M. Thurner and S. Selberherr, Three-dimensional effects due to the field oxide in MOS devices analyzed with MINIMOS 5, *IEEE Trans. Computer-Aided Design*, CAD-9(8) (1990) 856–867.

[9] K. Blotekjaer, Transport equations for electrons in two-valley semiconductors, *IEEE Trans. Electron Devices*, ED-17(1) (1970) 38–47.

[10] P.T. Landsberg and S.A. Hope, Two formulations of semiconductor transport equations, *Solid-State Electronics*, 20 (1977) 421–429.

[11] G. Baccarani and M.R. Wordeman, An investigation of steady-state velocity overshoot in silicon, *Solid-State Electronics*, 28(4) (1985) 407–416.

[12] M. Rudan and F. Odeh, Multi-dimensional discretization scheme for the hydrodynamic model of semiconductor devices, *COMPEL*, 5(3) (1986) 149–183.

[13] R.K. Cook and J. Frey, An efficient technique for two-dimensional simulation of velocity overshoot effects in Si and GaAs devices, *COMPEL*, 1(2) (1982) 65–87.

[14] Y.K. Feng and A. Hintz, Simulation of submicrometer GaAs MESFET's using a full dynamic transport model, *IEEE Trans. Electron Devices*, 35(9) (1988) 1419–1431.

[15] D. Chen, E.C. Kan, U. Ravaioli, C.W. Shu and R.W. Dutton, An improved energy transport model including nonparabolicity and non-Maxwellian distribution effects, *IEEE Electron Device Lett.* 13(1) (1992) 26–28.

[16] H. Lin, N. Goldsman and I.D. Mayergoyz, An efficient deterministic solution of the space-dependent Boltzmann transport equation for silicon, *Solid-State Electronics*, 35(1) (1992) 33–42.

[17] K. Hennacy, N. Goldsman and I.D. Mayergoyz, 2-dimensional solution to the Boltzmann transport equation to arbitrarily high-order accuracy, *Proc. Int. Workshop on Computational Electronics*, Leeds, 1993, 118–122.

[18] D. Ventura, A. Gnudi and G. Baccarani, Multi-dimensional spherical harmonics expansion of Boltzmann equation for transport in semiconductors, *Appl. Math. Lett.*, 5(3) (1992) 85–90.

[19] A. Gnudi, D. Ventura and G. Baccarani, Two-dimensional MOSFET simulation by means of a multidimensional spherical harmonics expansion of the Boltzmann transport equation, *Solid-State Electronics*, 36(4) (1993) 575–581.

[20] M.V. Fischetti and S.E. Laux, Monte Carlo analysis of electron transport in small semiconductor devices including band-structure and space-charge effects, *Physical Rev. B,* 38(14) (1988) 9721–9745.
[21] D.Y. Cheng, C.G. Hwang and R.W. Dutton, PISCES-MC: A multiwindow, multimethod 2-D device simulator, *IEEE Trans. Computer-Aided Design,* 7(9) (1988) 1017–1026.
[22] F. Venturi, R.K. Smith, E.C. Sangiorgi, M.R. Pinto and B. Ricco, A general purpose device-simulator coupling Poisson and Monte Carlo transport with applications to deep submicron MOSFET's, *IEEE Trans. Computer-Aided Design,* 8(4) (1989) 360–369.
[23] J.M. Higman, K. Hess, C.G. Hwang and R.W. Dutton, Coupled Monte Carlo–drift diffusion analysis of hot-electron effects in MOSFET's, *IEEE Trans. Electron Devices,* 36(5) (1989) 930–937.
[24] H. Kosina and S. Selberherr, A hybrid device simulator that combines Monte Carlo and drift-diffusion analysis, *IEEE Trans. Computer-Aided Design,* 13(2) (1994) 201–210.
[25] K. Hess, *Advanced Theory of Semiconductor Devices,* Prentice Hall, 1988.
[26] S. Selberherr, *Analysis and Simulation of Semiconductor Devices,* Springer, 1984.
[27] M. Rudan and A. Gnudi, The hydrodynamic model of current transport in semiconductors, *Euro. School on Device Modeling, University of Bologna, Italy,* 1991, 125–160.
[28] H.K. Gummel, A self-consistent iterative scheme for one-dimensional steady state transistor calculations, *IEEE Trans. Electron Devices,* ED-11 (1964) 455–465.
[29] D.M. Caughey and R.E. Thomas, Carrier mobilities in silicon empirically related to doping and field, *Proc. IEEE,* 52 (1967) 2192–2193.
[30] S. Selberherr, W. Hänsch, M. Seavey and J. Slotboom, The evolution of the MINIMOS mobility model, *Solid-State Electronics,* 33(11) (1990) 1425–1436.
[31] M. Ali-Omar and L. Reggiani, Drift and Diffusion of charge carriers in silicon and their empirical relation to the electric field, *Solid-State Electronics,* 30(7) (1987) 693–697.
[32] C. Canali, G. Majni, R. Minder and G. Ottaviani, Electron and hole drift velocity measurements in silicon and their empirical relation to electric field and temperature, *IEEE Trans. Electron Devices,* ED-22 (1975) 1045–1047.
[33] C. Canali and G. Ottaviani, Saturation values of the electron drift velocity in silicon between 300K and 4.2K, *Physics Lett.,* 32A(3) (1970) 147–148.
[34] P.C. Dhanasekaran and B.S.V. Gopalam, The physical behaviour of an n+p silicon solar cell in concentrated sunlight, *Solid-State Electronics,* 25(8) (1982) 719–722.
[35] J. Dziewior and W. Schmid, Auger coefficients for highly doped and highly excited silicon, *Appl. Phys. Lett.,* 31 (1977) 346–348.
[36] A.G. Chynoweth, Ionization rates for electrons and holes in silicon, *Physical Rev.,* 109 (1958) 1537–1540.
[37] C.R. Crowell and S.M. Sze, Temperature dependence of avalanche multiplication in semiconductors, *Appl. Phys. Lett.,* 9 (1966) 242–244.
[38] D.R. Decker and C.N. Dunn, Temperature dependence of carrier ionization rates and saturated velocities in silicon, *J. Electronic Mat.,* 4(3) (1975) 527–547.
[39] Y. Okuto and C.R. Crowell, Ionization coefficients in semiconductors: a nonlocalized property, *Physical Rev. B,* 10 (1974) 4284–4296.
[40] G. Baccarani, M. Rudan, R. Guerrieri and P. Ciampolini, Physical models for numerical device simulation, *Euro. School on Device Modeling, University of Bologna, Italy,* 1991, 1–70.
[41] H.J. Peifer, B. Meinerzhagen, R. Thoma and W.L. Engl, Evaluation of impact ionization modeling in the framework of hydrodynamic equations, *Int. Electron Devices Meeting,* 1991, 131–134.
[42] W. Quade, E. Schöll and M. Rudan, Impact ionization within the hydrodynamic approach to semiconductor transport, *Solid-State Electronics,* 36(10) (1993) 1493–1505.
[43] W. Scheonmaker and R. Vankemmel, A numerical implementation of the energy balance equations based on physical considerations, in S. Selberherr, H. Stippel and E. Strasser, editors, *Simulation of Semiconductor Devices and Processes,* Springer-Verlag, 1993, 117–120.
[44] A. Forghieri, R. Guerrieri, P. Ciampolini, A. Gnudi, M. Rudan and G. Baccarani, A new discretization strategy of the semiconductor equations comprising momentum and energy balance, *IEEE Trans. Computer-Aided Design,* 7(2) (1988) 231–242.
[45] T.W. Tang, Extension of the Scharfetter–Gummel algorithm to the energy balance equation, *IEEE Trans. Electron Devices,* ED-31(12) (1984) 1912–1914.
[46] A. Leone, A. Gnudi and G. Baccarani, Hydrodynamic simulation of an n-MOSFET at 77K, in H.E. Maes, R.P. Mertens and R.J. Van Overstraeten, editors, *22nd European Solid State Device Research Conference,* Leuven, 1992, 291–294.
[47] W. Hänsch, The drift-diffusion equation and its applications in MOSFET modeling, in *Computational Microelectronics,* Springer-Verlag, 1991.
[48] B. Meinerzhagen and W.L. Engl, The influence of the thermal equilibrium approximation on the accuracy of classical two-dimensional numerical modeling of silicon submicrometer MOS transistors, *IEEE Trans. Electron Devices,* 35(5) (1988) 689–697.
[49] H. Kosina and S. Selberherr, Efficient coupling of Monte Carlo and drift diffusion method with appli-

cations to MOSFETs, *22nd Conf. Solid State Devices and Materials,* Sendai, 1990, 139–142.
[50] S.C. Lee and T.W. Tang, Transport coefficients for a silicon hydrodynamic model extracted from inhomogeneous Monte-Carlo calculations, *Solid State Electronics,* 35(4) (1992) 561–569.
[51] M.A. Stettler, A. Das and M.S. Lundstrom, Self-consistent solution of the Boltzmann transport equation using the scattering matrix approach, in W. Fichtner and D. Aemmer, editors, *Simulation of Semiconductor Devices and Processes,* Hartung-Gorre, 1991, 215–221.
[52] M.A. Stettler, M.A. Alam and M.S. Lundstrom, A critical examination of the assumptions underlying macroscopic transport equations for silicon devices, *IEEE Trans. Electron Devices,* 40(3) (1993) 733–740.
[53] W. Hänsch and M. Miura-Mattausch, The hot-electron problem in small semiconductor devices, *J. App. Physics,* 60(2) (1986) 650–656.
[54] R. Thoma, A. Emunds, B. Meinerzhagen, H.J. Peifer and W.L. Engl, Hydrodynamic equations for semiconductors with nonparabolic band structure, *IEEE Trans. Electron Devices,* 38(6) (1991) 1343–1353.
[55] H.L. Grubin and J.P. Kreskovsky, Quantum moment balance equations and resonant tunneling structures, *Solid-State Electronics,* 32(12) (1989) 1071–1075.
[56] C.L. Gardner, The classical and quantum hydrodynamic models, *Proc. Int. Workshop on Computational Electronics,* Leeds, 1993, 25–36.
[57] J.R. Zhou and D.K. Ferry, Simulation of ultra-small GaAs MESFET using quantum moment equations, *IEEE Trans. Electron Devices,* 39(3) (1992) 473–478.
[58] S. Bandyopadhyay, M.E. Klausmeier-Brown, C.M. Maziar, S. Datta and M. Lundstrom, A rigorous technique to couple Monte Carlo and drift-diffusion models for computationally efficient device simulation, *IEEE Trans. Electron Devices,* ED-34(2) (1987) 392–399.
[59] R.W. Hockney and J.W. Eastwood, *Computer Simulation Using Particles,* Adam Hilger, 1988.
[60] G.A. Sai-Halasz and H.B. Harrison, Device-grade ultra-shallow junction fabricated with antimony, *IEEE Electron Device Lett.* EDL-7(9) (1986) 534–536.
[61] G.A. Sai-Halasz, M.R. Wordeman, K.P. Kern, E. Ganin, S. Rishton, D.S. Zicherman, H. Schmid, M.R. Polcari, H.Y. Ng, P.J. Restle, T.H. Chang and R.H. Dennard, Design and experimental technology for 0.1 – μm gate length low-temperature operation FET's, *IEEE Electron Device Let.,* EDL-8(10) (1987) 463–466.
[62] C. Jacoboni and L. Reggiani, The Monte Carlo method for the solution of charge transport in semiconductors with applications to covalent materials, *Rev. Modern Physics,* 55(3) (1983) 645–705.
[63] Chu-Hao, J. Zimmermann, M. Charef, R. Fauquembergue and E. Constant, Monte Carlo study of two-dimensional electron gas transport in Si-MOS devices, *Solid State Electronics,* 28(8) (1985) 733–740.